

THE ACTIVE CRUSTAL DEFORMATION FIELD OF THE AEGEAN AREA INFERRED FROM SEISMICITY AND GPS DATA

C.B. Papazachos

Geophysical Laboratory, University of Thessaloniki, PO Box 352-1, GR-54006 Thessaloniki, GREECE. (costas@lemnos.geo.auth.gr)

Abstract. A model is derived for the deformation velocity and strain rate field of the broader Aegean area, using the most reliable available seismological and GPS data. The data are initially processed separately in order to define a continuous velocity field using polynomial fits to the original data and the obtained results show a very good agreement for the two data sets. Using this result, seismological and GPS data are jointly interpreted assuming that the seismic deformation represents a part of the total deformation, revealed by the GPS data and a common seismic-GPS deformation field is defined through a non-linear iterative process. The obtained seismic-to-total deformation ratio shows that in the strike-slip faulting areas (North Aegean Trough and Cephalonia) almost all deformation is expressed seismically, whereas the corresponding values are significantly smaller (around 20-40%) throughout the remaining Aegean area where normal faulting dominates. The final jointly determined deformation field is more detailed than previous estimations and further supports the idea that the Aegean should not be considered as a part of a single Anatolia-Aegean microplate, which has been suggested to perform an almost rigid body rotation. The rotational component of the obtained velocity field, shows a clockwise rotation in central and SW Aegean and an anticlockwise rotation in the SE Aegean, in very good agreement with the available palaeomagnetic data. A modified kinematic-tectonic model is presented for the Aegean, using the final deformation field, as well as the seismological and GPS information used in the study.

1. Introduction

Active crustal deformation studies have traditionally relied on the use of earthquake data. *Kostrov* (1974) was the first to demonstrate how one can extend the simple principle of *Brune* (1968) and estimate strain rates for a seismogenic volume from moment tensors. *Molnar* (1979) and *Jackson and McKenzie* (1988) continued this analysis and demonstrated how deformation velocities can be calculated on the basis of certain assumptions. *Papazachos and Kiratzi* (1992) showed how the moment tensors could be used only for the estimation of the pattern of deformation, leaving the magnitude of the deformation to be determined from the more complete seismicity record. Following the ideas of *Haines* (1982) who estimated horizontal velocity fields using geodetic observations of shear strain rates, *Holt et al.* (1991) and *Holt and Haines* (1993) demonstrated how the velocity field could be obtained if average strain rates were determined from moment tensor data using the *Kostrov* (1974) formulation.

During the last decade, GPS measurements over regional distances have reached the desired accuracy and provide independent estimates of the total horizontal crustal deformation, which can be directly compared with the seismological results. These comparisons are very important in order to assign the compatibility between the two data sets. Both types of data have different sources of ambiguity: Seismicity results often have large errors mainly due to the uncertainty in the seismic moment and the completeness of the seismicity record (*Papazachos and Kiratzi*, 1992), while GPS data sometimes express movements of surficial layers that do not reflect the true deformation of the whole crust. Moreover, seismological data usually cover a much longer period (typically hundreds of years) than the GPS data, which span a much shorter time-interval (typically up to 5-15 years). The most important aspect of this problem is that seismological data only provide the part of the crustal deformation, which is expressed seismically, while GPS observations are controlled by the total deformation. Therefore, this comparison allows the estimation of an "efficiency index", that is, the spatial distribution of the seismic to total deformation ratio.

In the present paper the active crustal deformation field of the Aegean area is examined, as obtained from both seismological and GPS data. The results from these data sets are compared and combined in order to determine the main characteristics of deformation for the examined area. The method followed is similar to that of *Holt et al.* (1991) and *Holt and Haines* (1993), extended in order to also incorporate GPS velocity data. The main modification, as far as the seismological estimates are concerned, is the incorporation of a more detailed data set for the moment tensors and the use of a new moment rate release distribution for the area based on recent results (*Papazachos*, 1999a). The improved new data allow a more detailed study of the active (seismic) deformation field for the Aegean area. For the GPS observations a database has been compiled using the results published in previous studies. This data set has been processed in a similar way with the seismological data. The final comparisons are performed for both the strain rate and the velocity field. A Monte-Carlo approach is used to model the error propagation in the determined results. Finally, a unified deformation field is determined from the joint interpretation of both data-sets, as well as an estimation of the spatial distribution of the "efficiency index" (ratio of seismic to total deformation) is presented for the Aegean area. Moreover, the obtained rotational component of the velocity field from both seismicity and GPS data is computed and compared with palaeomagnetic estimates, showing a very good agreement. Appropriate error estimates are computed for all

model parameters using the same Monte-Carlo approach.

2. Active Tectonics of the Aegean Area

The Aegean area (Figure 1) has always received a wide attention from many scientists, regarding various aspects of different geosciences. In several cases, fundamental results have been obtained in the Aegean regarding various geological-geophysical topics, such as basin formation processes due to lithospheric stretching, etc. A detailed presentation of such results can be found in *Jackson (1994)*. The main reason behind this natural geophysical-geological observatory is the high deformation rates observed in the area, the highest in the whole Africa-Eurasia collision zone. More than 60% of the European seismicity, which is the most prominent manifestation of this deformation, is expressed here with earthquakes with magnitudes up to $M_W=8.2$ (*Papazachos, 1990*). This deformation is associated with the subduction of the eastern Mediterranean lithosphere (see figure 1) under the Aegean along the Hellenic Arc (*Papazachos and Comninakis, 1969; Papazachos and Delibasis, 1969; Le Pichon and Angelier, 1979*) and the westward motion of Anatolia along the North Aegean Fault (*McKenzie, 1970, 1972; Taymaz et al., 1991*) and its continuation in the Aegean along the North Aegean Trough. The Aegean exhibits the typical characteristics of a marginal sea, with high heat flow (*Fytikas et al., 1985*), volcanic activity along its volcanic arc (*Georgalas, 1962*) and high magnetic and positive gravity isostatic anomalies (*Voght and Higgs, 1969; Makris, 1976, 1978*).

Shallow seismicity extends throughout the whole Aegean back-arc area, mainly associated with normal faults (*McKenzie, 1978*), except the North Aegean Trough and the Cephalonia Fault which is the contact between the Eastern Mediterranean and Adriatic plates (*Scordilis et al., 1985*) where dextral strike-slip faults are observed. Of course dextral strike-slip faults due to the Anatolia motion, are also observed in the Aegean much further south than the North Aegean Trough (*Taymaz et al., 1991; Papazachos et al., 1999b*). Along the Hellenic Arc, the subduction results in a high shallow seismicity with low-angle thrust faults (e.g. *Papazachos, 1990*). The subduction is clearly identified both by large scale (*Spakman, 1988*) and local (*Papazachos and Nolet, 1997*) tomographic studies, as well as by the high intermediate-depth seismicity which is expressed along a well-defined Benioff zone (*Papazachos and Comninakis, 1969, 1971, Papazachos et al., 2000*).

This complicated geotectonic setting motivated a number of studies regarding the active crustal deformation of the area. For the outer Hellenic Arc various values have been published for the crustal shortening rate at different segments of the Arc, ranging between 5-30mm/yr, with an average value of ~ 10 mm/yr (*Jackson and McKenzie, 1988; Papazachos and Kiratzi, 1996*). For the back-arc area extension velocities have been estimated for different seismogenic volumes (*Tselentis and Makropoulos, 1986; Jackson and McKenzie, 1988; Ekström and England, 1989; Papazachos and Kiratzi, 1992, 1996*). In summary, the results show an average almost N-S extension of the order of 30mm/yr for the whole Aegean area (*Papazachos and Kiratzi, 1996*). *Jackson et al. (1992)* used the methodology of *Holt et al. (1991)* and *Holt and Haines (1993)* and estimated a continuous horizontal velocity field using local estimates of the strain rate from moment tensor summation over a 1.5° grid covering the central and eastern part of the Aegean area. Using a smooth fifth-order polynomial function to approximate the velocity field, they estimated its main characteristics, as well as the expected fault directions and fault rotations predicted by this velocity field. Furthermore, they have found a clockwise rotating field throughout the whole Aegean area and explained how it was possible to obtain both clockwise and anticlockwise block rotations in the same clockwise rotating velocity field.

Recently, high accuracy GPS data have been collected in a large number of field experiments (*Biliris et al., 1991; Oral, 1994; Kahle et al., 1995; Reilinger et al., 1997; Clarke et al., 1998; Straub et al., 1997; McClusky et al., 2000*) for the Aegean area. In general, the deformation pattern predicted by the GPS data seems to be compatible with previous results inferred from seismicity. A typical example is the existence of a narrow zone where E-W extension is observed, which lies between the thrust-fault of the outer Hellenic Arc and the N-S extension field of the back-arc area. This zone has been identified using fault plane solutions (*Papazachos et al., 1984, 1998; Kiratzi et al., 1987*) and was confirmed by recent GPS measurements (*McClusky et al., 2000*).

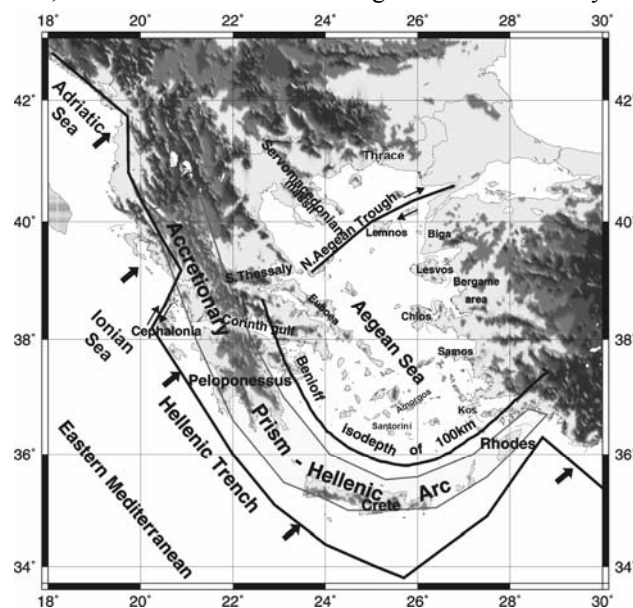


Figure 1. General features of tectonic origin of the broader Aegean area.

3. Estimation of the Velocity and Strain Rate Field From Seismicity and GPS Data for the Aegean Area

In his pioneering work, (Kostrov, 1974) showed that the strain tensor, ε , of a deforming volume, V , where N earthquakes have occurred with corresponding moment tensors, M^n , could be estimated by:

$$\varepsilon_{ij} = \frac{1}{2\mu V} \sum_{n=1}^N M_{ij}^n \quad (1)$$

In order to use equation (1) a complete sample of all large events and their corresponding moment tensors for a large enough time period is necessary. Unfortunately, moment tensors are only available for the last ~30-40 years and usually the corresponding data sets are not complete even for this short period. Moreover, it is questionable if this time interval is large enough in order to be representative of the deformation field. On the other hand, the seismicity record is usually much more complete, especially for large events, i.e. for the Aegean area is of the order of few hundreds of years for the less active areas. Papazachos and Kiratzi (1992) suggested that the "magnitude" of the deformation could be estimated from the seismicity record through the annual moment rate, \dot{M}_0 , and the "pattern" of the deformation could be estimated from the available fault plane solutions. These fault plane solutions do not have to be complete in time, i.e. solutions for historical events can also be included. Using this formulation, equation (1) can be transformed to:

$$\dot{\varepsilon}_{ij} = \frac{1}{2\mu V} \dot{M}_0 \bar{F}_{ij} \quad (2)$$

where F is the "representative focal mechanism tensor", which is given by:

$$\bar{F}_{ij} = \sum_{n=1}^N M_{ij}^n / \sum_{n=1}^N M_0^n \quad (3)$$

where M_{ij}^n and M_0^n are the moment tensor and the scalar moment for each available fault plane solution, respectively (Papazachos and Kiratzi, 1992). The annual moment rate, \dot{M}_0 , in equation (2) can be estimated independently from the seismicity record. In the present study we use Molnar's (1979) formulation:

$$\dot{M}_0 = \frac{A}{1-B} \bullet M_{0,max}^{1-B} \quad A = 10^{(a+\frac{bd}{c})}, \quad B = \frac{b}{c} \quad (4)$$

where $M_{0,max}$ is the moment of the maximum magnitude expected for this seismogenic volume, a and b are the constants of the Gutenberg-Richter relation and c and d are the constants of the scalar moment-moment magnitude relation:

$$\log M_0 = c M + d \quad (5)$$

Using this formulation, the strain rate can be efficiently estimated (e.g. Papazachos and Kiratzi, 1996), while the derivation of the deformation through the use of the moment rate, \dot{M}_0 , using equation (4a) allows for the incorporation of the effect of smaller earthquakes, which can account for a large percent of the total deformation rate. For example, in the Corinth gulf area and using the previously described formulation Papazachos and Kiratzi (1996) estimated a N-S extension of ~11mm/yr, whereas Ambraseys and Jackson (1997) estimated a similar rate of ~10mm/yr by doubling the rate calculated using only events with $M \geq 6.0$, in order to include the effect of smaller earthquakes.

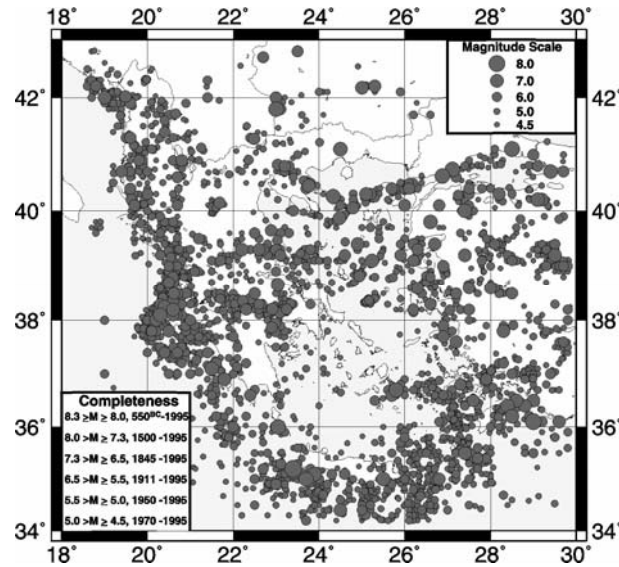


Figure 2. Earthquake epicenters for the period 550BC-1996 used in the present study. The completeness of the catalogue is also shown.

Jackson and McKenzie (1988) demonstrated that it is possible to estimate the velocity tensor using some assumptions for the dimensions of the deforming zone and its boundary conditions. They demonstrated that the main problem of this calculation stems from the fact that from the strain rate tensor we can only estimate the symmetric part of the velocity gradient tensor and not its antisymmetric part, which represents the rotational part of the deformation that can not be resolved due to the intrinsic limitations of the moment tensor which is symmetric. In order to overcome this problem, Holt et al. (1991) and Holt and Haines (1993) demonstrated that when the spatial variations of the

strain rate tensor are known, the complete velocity field can be recovered. This is accomplished by estimating a continuous velocity that fits the strain rate data. Then the velocity gradient tensor can be easily estimated

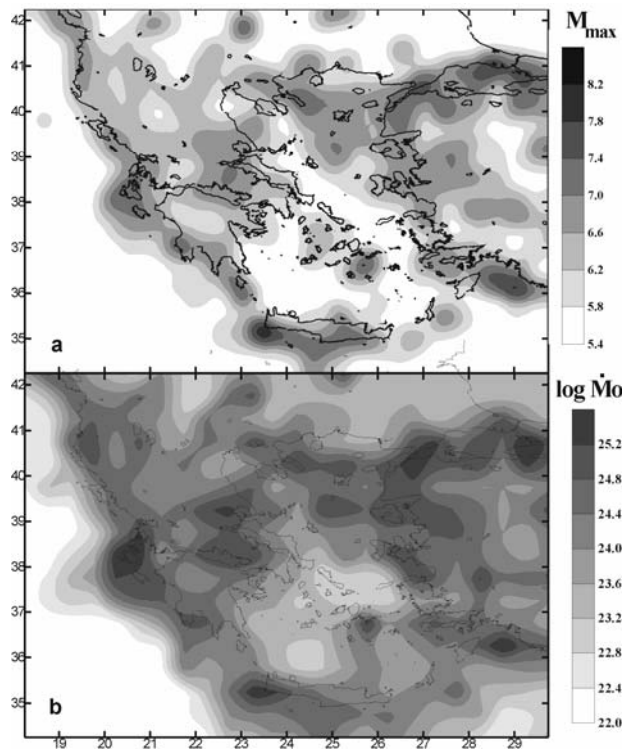


Figure 3. a) Geographical distribution of the maximum magnitude determined in the present study for the Aegean area. b) Same figure for the moment rate release. Notice the delineation of certain high seismicity areas (Hellenic Arc, Corinth gulf, southern Thessaly, etc.)

everywhere and therefore the vorticity of this field $\dot{\omega}$ is also recovered. The fitted velocity field is usually described by polynomial functions, which can be determined by an appropriate inversion scheme so that the difference between the predicted and observed (from seismicity) strain rates is minimized.

Haines and Holt (1993) extended their method for a spherical earth and used an elaborate inversion scheme that incorporates the possible sources of misfit between the predicted and observed strain rates. Jackson *et al.* (1992) applied this method for the central and eastern Aegean area, but since the size of the deforming area was less than 1000km, the flat earth approximation was employed. They separated the study area in a grid and estimated strain rates from the available fault plane solutions of large events using data from 1903 to 1983. In their analysis they showed that for the data set used, a fifth order polynomial and a grid separation of 1.5° was appropriate, whereas higher order polynomials or denser grids did not change the results or led to unrealistic spatial changes of the strain rate field.

In the present paper, we follow a modified procedure in order to estimate the velocity field of the Aegean area. For the estimation of strain rates from seismological data, we used the method of Papazachos and Kiratzi (1992) previously described. The other modifications concern the data set used, the estimation of strain rates from seismicity data (grid selection, etc.) and the incorporation of GPS

data in the analysis. Earthquake and GPS data are processed both independently and jointly, whereas a full error analysis incorporates a Monte-Carlo approach.

3.1 Seismicity Data and Estimation of Strain Rates

In order to estimate strain rates using equation (2), we need to estimate the moment rate distribution, as well as the fault plane solutions of the study area. For the moment rate estimation, equations (4) require that the a and b values, as well as the maximum magnitude for the seismogenic volume which is examined are available. If the seismogenic volume is very small, the estimation of these quantities using standard techniques might lead to results which are not representative of the true seismicity level in the area. For this reason, we used the results of Papazachos (1999a), who obtained estimates of the distribution of the a and b values for the Aegean area using a grid of 0.5° . The data set used was the new seismicity catalogue for the Aegean area (Papazachos *et al.*, 1997) for the period 550BC-1996. The completeness of this catalogue, which contains more than 3400 events with $M_W \geq 4.5$ and the corresponding epicenters are shown in figure (2). It is interesting to notice that the major seismicity areas are clearly identified in this map (North Aegean Trough, Hellenic Arc, Southern Thessaly basin, Corinth gulf, Cephalonia fault, etc.) The estimation of the a and b values (Papazachos, 1999a) is based on the traditional "mean value" method (Milne and Davenport, 1969) with the additional assumption that the b -value exhibits smooth spatial variations. The obtained b -value distribution for the Aegean is almost unchanged when instrumental or both instrumental-historical data are used, whereas the a -value distribution varies, depending on the spatial coherency imposed in the calculations. In the present study the a -value distribution determined with the lowest level of spatial coherency was used, as this computed in Papazachos (1999a), in order to impose the minimum level of "smoothing" in the seismic strain rate distribution, which is used in subsequent calculations.

A similar approach can be adopted in estimating the spatial variation of the maximum magnitude. For this purpose, no completeness criteria were applied but the full catalogue including both instrumental and historical seismicity data is used in order to estimate a smooth distribution of the expected maximum magnitude for the same 0.5° grid covering the Aegean area, using a procedure similar to the one applied for the b -value distribution. The final distribution of the maximum expected magnitude, M_{max} , is shown in figure (3a). Clearly the obtained values are strongly affected mainly by the large historical events, which can be recognized in some areas as smooth high-magnitude "spots". However, this is not necessarily misleading as these large events have contributed significantly in the released moment rate and their effect is incorporated in Molnar's equation (4a). On the other hand, this imposes certain limitations on the accuracy of the obtained moment-rate release, as also

indicated by Molnar (1979). Papazachos and Kiratzi (1992) also pointed it out this problem though a detailed error analysis of equation (4a), a point which will be discussed later in the corresponding error analysis.

Using equation (4a), the final moment rate release distribution, \dot{M}_0 , has been estimated and is shown in figure (3b). Clearly this moment rate map preserves the signature of the major rupture zones identified by high-seismicity areas of figure (2) and quantifies the seismic energy release for each zone. The obtained moment rate values are in very good agreement with estimates independently obtained for various seismic zones in the Aegean (e.g. Papazachos and Kiratzi, 1996).

For the fault plane solutions, the available data sample concerns a much smaller time period for which reliable solutions are available. As a basis for this data set we have used the 127 fault plane solutions listed by Papazachos and Papazachou (1997) which correspond to shallow events ($h \leq 60\text{km}$) up to 1995 with equivalent moment magnitude $M \geq 5.5$ and have been defined by waveform modeling or first motions of long-period recording for older events. This data set has been updated to include the corresponding events up to 2000, as well as some recent smaller events ($M_w \geq 5.3$) for which reliable waveform modeling fault-plane solutions were available. Also, observations for 10 large events ($M \geq 6.7$) for which information from surface ruptures was available (also listed by Papazachos and Papazachou (1997)) were also used, resulting in a final data set of 186 fault plane solutions. These fault plane solutions are presented in figure (4), where they are divided into four main groups, on the basis of their faulting type and fault orientation.

The first group (figure 4a) includes all thrust faults, which are found along the Hellenic Arc and their continuation north of the Cephalonia fault along the western coast of northern Greece, Albania and Montenegro (see figure 1). The presence of these thrust faults is clearly associated with the subduction of the eastern Mediterranean beneath the Aegean (Papazachos and Delibasis, 1969) and the continental-continental type collision of the Adriatic (Apulia) microplate with the western Greek-Albanian coasts (Anderson and Jackson, 1987).

The second group of fault-plane solutions (figure 4b) includes all strike-slip faults, which are located in two areas. The first area covers the westernmost section of the North Anatolian Fault and its continuation along the North Aegean Trough, where dextral strike-slip faulting dominates (McKenzie, 1970, 1972; Taymaz et al., 1991). This dextral strike-slip zone appears to be interrupted along the Greek mainland

and to continue in the area of the Cephalonia fault (Scordilis et al., 1985). Recently, similar faulting has been proposed for the NW Peloponnesus area (Papazachos et al., 1998, 1999). The possible existence and extent of dextral strike-slip faulting on the Greek mainland, as well as in the southern Aegean is still an open question, although large strike-slip events have not been observed in these areas.

The third and fourth group of faults (figure 4c and 4d) both correspond to normal faults. In figure (4c) a narrow zone of almost N-S oriented normal faults can be identified, which more or less runs parallel to the thrust fault zone (figure 4a) at an average distance of 50-70km. The presence of this zone is clearly related to the subduction-collision tectonics of the thrust-fault zone and several mechanisms have been proposed for its existence (e.g. Armijo et al. (1992)). However, the largest part of the back-arc Aegean area is dominated by normal faults which have an E-W trend on the average. This zone extends from southern Aegean all the way up to southern Bulgaria and partly overlaps with the dextral strike-slip fault zone in the northern Aegean.

In order to determine the spatial variation of the fault-plane solutions, the corresponding moment-tensor elements and the stress field we have followed the approach of Papazachos et al. (1999) who used fault plane solutions for 52 large events, as well as surface fault traces, macroseismic data, and clustering of small events to

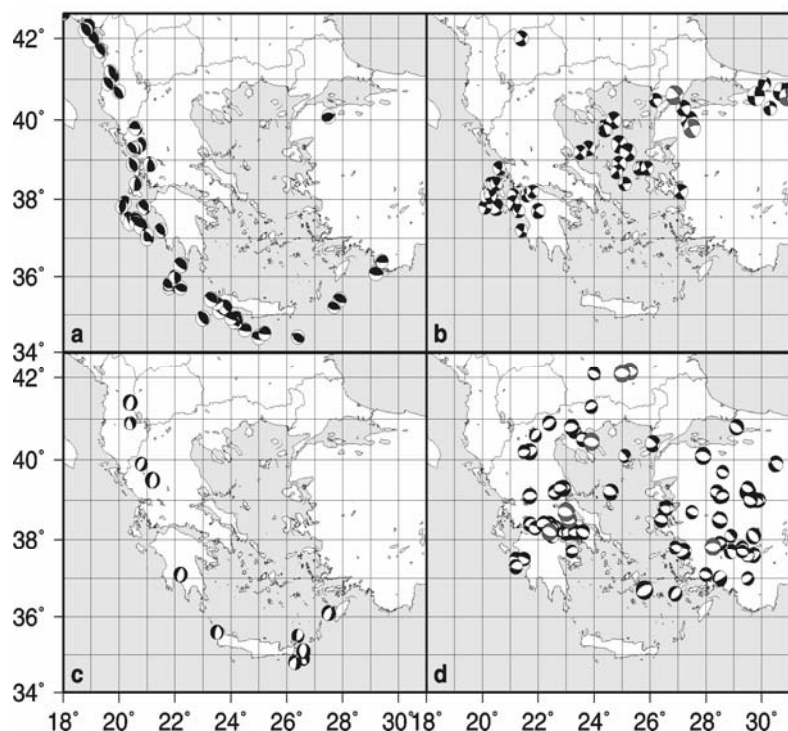


Figure 4. Spatial distribution of the 186 fault plane solutions used in the present study: a) Thrust fault plane solutions, b) Strike-slip fault plane solutions, c) Normal fault plane solutions corresponding to approximately N-S trending faults, and d) Normal fault plane solutions corresponding to approximately E-W trending faults.

define the rupture zones of 150 large shallow events in the Aegean area since 426BC. Using these rupture zones, they defined the stress field for 36 "clusters" which show a coherent stress field. Using the information presented in their work, as well as the much larger data-set of fault plane solutions previously mentioned we have modified their results and recalculated the average stress-field characteristics for 39 clusters. The typical fault plane solutions which correspond to the obtained stress field are shown in figure (5a), while the corresponding information (cluster location, P and T axes) of each cluster is shown in Table (1).

In order to determine the strain rate, it was necessary to regionalize this stress field and estimate the stress field for the same 0.5° grid for which moment rates were available. For this reason, all the previously described fault plane solutions for the Aegean area were used, in addition to the existing information provided by Papazachos *et al.* (1999). Moreover, for areas where the data coverage was relatively poor additional

information from microseismicity (e.g. Hatzfeld *et al.*, 1988), neotectonic (e.g. Pavlidis, 1996; Doutsos and Kokkalas, 2001) and geomorphological data were also taken into account.

The final distribution of the stress field in the Aegean area is shown in Figure (5b). Since in this figure the horizontal projections of the P- and T-axes are plotted, in several cases the axes orientations are not normal. Cells for which no fault plane solutions were available are shown either in light-gray (quite reliable) or in dark-gray (less reliable), depending on the amount and quality of additional information which has been used in order to associate each cell with one of the defined stress-field clusters. For instance, in cases when a cell was located along a well-defined seismic zone, e.g. along the North Aegean Trough for which seismological, neotectonic, historical, macroseismic and geomorphological information show the existence of strike-slip faulting, the stress-field was determined from the neighboring cells and was considered as relatively reliable (light-gray color in figure 4b). For several cells for which seismicity level is very low and no reliable information could be used the stress axes have not been defined.

It should be pointed out that the stress-field presented in figure (5b) is defined using the eigenvalues of the averaged unit-scaled moment tensors of the corresponding fault-plane solutions, calculated using the relations of Aki and Richards (1980). The estimation of this "representative focal mechanism tensor", F , for each cell as described by Papazachos and Kiratzi (1992) and used in the present work does not involve any inversion scheme for the determination of the spatial distribution of tresses (e.g. Gephart and Forsyth, 1984). The main reason for this approach is that the modification of Kostrov's method employed in the present study essentially relies on moment tensor and not stress-field information, hence figure (5) practically corresponds to the spatial distribution of the eigenvalues of the unit-scaled

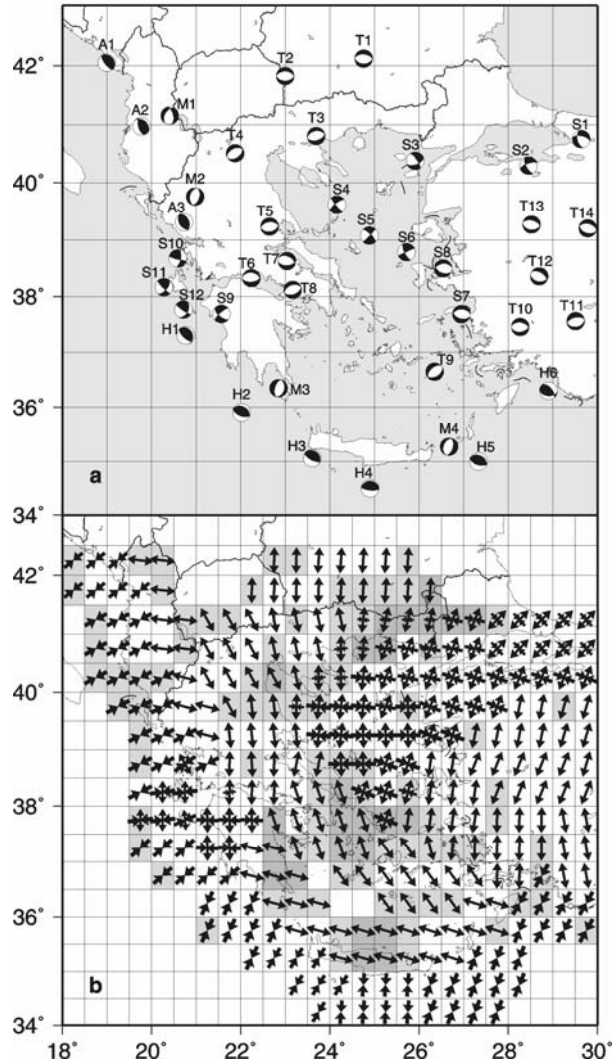


Figure 5. a) Stress field for the 39 clusters determined for the Aegean area (modified from Papazachos *et al.*, 1999). b) Geographical distribution of the stress field after regionalization of the previous figure for the 0.5° grid used in the present study.

average moment tensor, F . Moreover, the complexity of the active tectonics of the area and the faulting pattern revealed by figure (4) suggests that it is better to proceed in the regionalization of the stress field distribution through a careful data examination and joint evaluation with independent information (neotectonic, geomorphological, etc.), as is done by Papazachos and Kiratzi (1992, 1996), Papazachos *et al.* (1998, 1999) and in the present work.

The distribution of the moment rate (figure 3b) and the stress field (figure 5b) can be used in order to estimate the final variation of the strain rate in the Aegean area. For each cell the "representative focal mechanism tensor", \bar{F} , can be estimated using the relations of Aki and Richards (1980). Using equation (2), the

strain rate tensor can be computed for each grid cell using the corresponding values of \bar{F} and \dot{M}_0 . We should point out that the cells of very low seismicity where no data were available and the stress field was not determined (see figure 5b) have no influence on our calculations as they correspond to zero-strain cells. Hence, the strain-rate tensor was set to zero for these cells, which corresponds to a simple "transfer" of the velocity field across the cell borders. In total, the strain rate was determined for 307 out of the 408 grid cells defined for the Aegean area.

For all the previous computations, a grid of 0.5° was selected. There are two reasons for the selection of such a small grid size. The first reason is that the data set used in the present study is much larger than previous

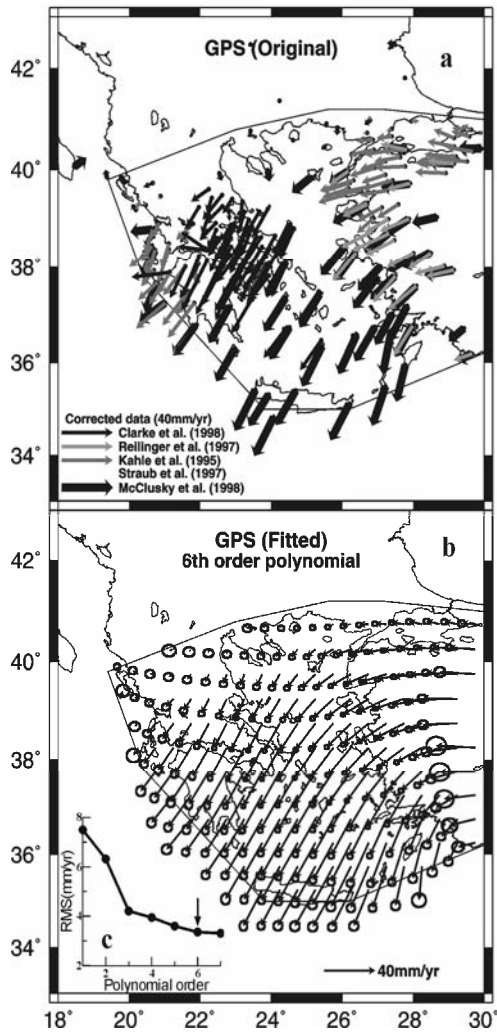


Figure 6. Comparison between the observed (a) and polynomially fitted (b) velocity field of GPS measurements for the broader Aegean region. The predicted velocity field and the corresponding 1-sigma errors are only shown for areas where original GPS observations were available. (c) Misfit of the polynomially fitted velocity field as a function of polynomial degree. A $N=6$ order polynomial was finally adopted.

Pichon et al., 1995; Oral et al., 1995; Kahle et al., 1998; Papazachos, 1999b; McClusky et al., 2000). The Aegean area is moving towards the SW, relative to Europe. The deformation velocities increase significantly from the western coasts of Turkey towards the southern Aegean. This increase can be attributed to the N-S extension in the Aegean area, which is probably caused by the slab-pull forces of the subducting Eastern Mediterranean lithosphere under the Aegean. Although, GPS observations from Turkey suggest that the Turkish microplate (Anatolia) performs a rigid body rotation (Oral, 1994; Oral et al., 1995; Reilinger et al., 1997) recent work based on seismological and GPS data (Papazachos, 1999b; McClusky et al., 2000) shows that the southern Aegean performs a roughly translational motion towards the S-SW, as is shown in figure (6a).

studies. The larger and more detailed data set allows us to retrieve smaller scale features of the velocity field, as is presented in the subsequent analysis. The second reason is that due to the large time span of the data and the procedure, which allows for a reliable estimation of the seismicity distribution, the results for a cell of 0.5° are robust. Therefore, they are more likely to represent the long-term characteristics of the deformation field, without losing most of its detailed features.

3.2 GPS data

A variety of geodetic experiments using GPS have been conducted in the Aegean and surrounding area in the last decade (Oral, 1994; Straub, 1996; Kahle et al., 1995; Reilinger et al., 1997). The original data were not homogeneous with respect to the way they were processed or their reference sites which have been adopted for the final solution. As a result, velocities relative to Europe refer to either Onsala (Sweden) or to Wettzell (Germany), depending on the specific choice of each study. However, if we take into account that the internal deformation in Europe and between Wettzell and Onsala is very small, as well as the observation that the magnitude of the reported velocities from these studies is relatively large (5-45mm/yr), we can conclude that any errors regarding the choice of the reference site in Europe are not significant, as has been also shown by Papazachos (1999b).

Recently, McClusky et al. (2000) reprocessed original data from various GPS campaigns and presented a large number of GPS velocity vectors for the whole eastern Mediterranean, including the broader Aegean area. Although the results presented in this work overcome the limitations of the reference system etc. previously mentioned, a significant number of GPS sites from previous studies were not included. For this reason, we have used all previously published GPS results and created a unified GPS dataset, using the McClusky et al. (2000) dataset as a reference system where all individual GPS data sets have been adapted by appropriate transformation, similar to the approach adopted in previous GPS studies e.g. Kahle et al. (1998). The unified GPS data set, shown in figure (6a), is compatible with the main features of the velocity field defined using GPS and earthquake data, as it has been presented for the whole Aegean area in previous studies (e.g. Jackson et al., 1992; Reilinger et al., 1997; Le

3.3 Obtaining a Continuous Strain Rate and Velocity Field From Seismological and GPS Data

In the previous sections, a discontinuous stress-strain rate (seismological) and velocity (GPS) field was presented for the Aegean area. In order to obtain a continuous field, we follow *Holt et al.* (1991) and *Holt and Haines* (1993) and use polynomial function to approximate the velocity field. Here, we simplify the analysis and use a simple planar latitude (φ) - longitude (λ) coordinate system. Since the latitude-longitude coordinate system does not have a uniform scale, we have instead adopted the corresponding Transverse Mercator coordinates, Northing (N_a) and Easting (E_a). The choice of the axes for this coordinate system is determined from the boundary conditions, which depend on the specific choice of the reference system. Since for the GPS data, all relative velocities refer to stable Europe, we have also chosen our reference system so that one axis lies on Europe. This axis (longitude) has been placed on the northern border of the study area, that is, at the latitude 43° N, where we assume that we have no deformation velocity relative to Europe, similar to previous studies (e.g. *Jackson et al.*, 1992). The other axis (Northing-approximately corresponding to latitude) was arbitrarily chosen to lie at the longitude of 18° E. Of course, some additional deformation may occur between the selected latitude and northern Europe where the GPS reference sites are located, but this deformation is very small compared to the corresponding deformation of the Aegean area. Moreover, contribution from different stress regimes (extension - compression) will result in the partial annealing even of this small deformation, hence practically eliminating any significant effect on our results.

Using this assumption, the velocity field for the Aegean area can be represented by polynomial function of degree N . Taking $x=E_a-E_a(\lambda=18^\circ)$ and $y=N_a(N_a(\varphi=43^\circ)-N_a)$, we can define the following relation for the two horizontal components of the velocity vector, u :

$$u_{x/y} = \sum_{k=1}^N \sum_{l=1}^k a_{kl}^{x/y} x^{k-l} y^l \quad (6)$$

Notice that all polynomial terms in equation (6) contain y in order to return a zero velocity at $y=0$ ($\varphi=43^\circ$). The constants $a_{kl}^{x/y}$ need to be defined in order to determine the continuous velocity field. From equation (6) we can estimate the following components of the strain rate tensor:

$$\dot{\epsilon}_{xx} = \frac{\partial u_x}{\partial x}, \quad \dot{\epsilon}_{yy} = \frac{\partial u_y}{\partial y}, \quad \dot{\epsilon}_{xy} = \frac{1}{2} \left(\frac{\partial u_x}{\partial y} + \frac{\partial u_y}{\partial x} \right) \quad (7)$$

Combining equations (6) and (7a,b,c) a complete expression for the $\dot{\epsilon}_{xx}$, $\dot{\epsilon}_{yy}$ and $\dot{\epsilon}_{xy}$ can be derived. Writing equations (7) for K grid cells, a linear system of $3K$ equations can be defined from the earthquake data ($\dot{\epsilon}_{xx}$, $\dot{\epsilon}_{yy}$ and $\dot{\epsilon}_{xy}$ determined from equation 2) from which we can determine the $N(N+1)/2$ unknown polynomial constants $a_{kl}^{x/y}$. Since usually $3K \gg N(N+1)/2$, the system is over-determined and it can be solved in the least-squares' sense.

For the geodetic data there are several methods for obtaining the velocity or strain rate field (e.g. *Moritz*, 1980). In the present study we extend the approach previously described to the estimation of a continuous velocity field from GPS velocity data. Therefore, equation (6) was used for the GPS data and a similar linear system was determined using the available GPS observations. For K GPS observations we have $2K$ linear constraints (velocities in equation 6) which are used to determine $N(N+1)/2$ polynomial coefficients and the corresponding linear system is similarly solved in the standard least-squares' sense. It should be also noted that for each GPS datum two equations are available (u_x and u_y) whereas for each strain rate datum (from earthquake information) three linear constraints (see equation (7a,b,c)) can be formed. Of course, once the polynomial coefficients are determined, equations (7a,b,c) can be applied to estimate the strain field from the GPS data.

For the Aegean area 234 GPS observations were used, while in several cases alternative estimates were available from different campaigns for the same site. However, the area covered by the available GPS observations was much smaller than for the results obtained from seismicity data as can be seen when comparing figures (5) and (6a). Since the determination of the velocity polynomial (equation 6) is essentially an optimization (fitting) problem in the least-squares' sense, the estimation of velocities outside the area covered by the GPS data corresponds to an extrapolation which can lead to large errors. For this reason the polynomial fit and the corresponding predicted velocities were restricted in the polygonal area shown in figure (6a), which is drawn by a solid line.

The velocity field, which was determined using the polynomial fit previously described is shown in Figure (6b) where velocities are only shown for the area inside the above mentioned polygonal area for which original GPS observations were available. The predicted velocities are shown for the same 0.5° grid for which moment rates are available and 1-sigma error ellipses are also shown for each velocity vector as they are calculated from the a posteriori covariance matrix of the least-squares solution. A $N=6$ order polynomial was selected for the fitted velocity field, as can be seen from the inset figure (6c), where the misfit (RMS) variation as a function of the polynomial order is shown, since for larger polynomial orders the misfit reduction was not significant. The comparison of figures (6a) and (6b) shows that a very good agreement between the observed and fitted velocities

can be observed. Moreover, figure (6c) shows that our smooth velocity field can fit the original GPS data with a remaining RMS misfit of 3mm/yr. This remaining misfit can be attributed to both errors in the original GPS data, as well as to the internal variability of the GPS data, which cannot be explained by smooth polynomial functions.

For the seismicity (strain rate) data the estimation of a continuous velocity field is not as straightforward as for the GPS data case. The main reason is that the errors involved in the estimation of strain rates (equation 2) can not be described by a simple covariance matrix. This problem arises from the fact that errors in \bar{F} are almost lognormal and can reach up to a factor of 2-3 (Papazachos and Kiratzi, 1992), while errors in \bar{F} are smaller but quite difficult to model. For this reason we followed a simple Monte-Carlo approach where random errors were introduced to these two components which are used in equation (2). For the moment-rate, \dot{M}_0 , which controls the deformation rate a lognormal distribution with a typical error of 200% was adopted (factor of 2), in accordance with Papazachos and Kiratzi (1992). For the components of \bar{F} a typical solid angle error of 10° was used for its eigenvectors, which corresponds to the principal stress components (P, T and Null axis) as previously explained. This error was chosen to increase to 20° and 30° for cells with no fault-plane solutions which have been determined to be more (light-gray in Figure 5b) or less (dark-gray in Figure 5b) reliable, as previously described. Although the choice of this increase of the typical error was made rather arbitrarily, larger values did not have important influence on our calculations as the corresponding cells are usually of lower seismicity (hence smaller strain-rates) and do not have a large contribution in the determination of the velocity field (equations 6 and 7). Using these error distributions we introduced random errors in \dot{M}_0 and \bar{F} and applied equation (2) for the strain rate estimation. This procedure was applied repeatedly (typically more than 2000 times) for each of the 307 cells shown in figure (5b) and the corresponding strain rate components were used in equation (7) for the determination of a unique velocity polynomial (equation 6), as previously described.

For the final estimations 921 linear constrains (strain-rate components) were available from the seismicity data. The determination of the 72 polynomial constants was performed using SVD and the standard least-squares' solution was determined. Haines and Holt (1993) use a sophisticated inversion scheme which takes into account the expected misfit between the observed and predicted strain rates, in order to determine the polynomial coefficients of equation (6). However, the motivation behind such an inversion technique was the fact that in their studies the estimated strain rates usually referred to large scale areas and often the strain rate was assumed to be constant for regions of varying size, which are expected to have different influence on the final solution. For the Aegean, the data set of Jackson *et al.* (1992) exhibited gaps in the areas where e.g. no fault plane solutions were available. In the present study we do have such difficulties: the size of all grid cells is the same and the data set is significantly larger which results in a dense coverage of the study area. Therefore, the simple least-squares' inversion is adequate and no special damping-smoothing constraints need to be added in the final linear system. It should also be pointed out that such constraints were already implicitly used in the seismicity parameter calculation (Papazachos, 1999a), which is the most important estimation as it affects the size of the deformation in each cell.

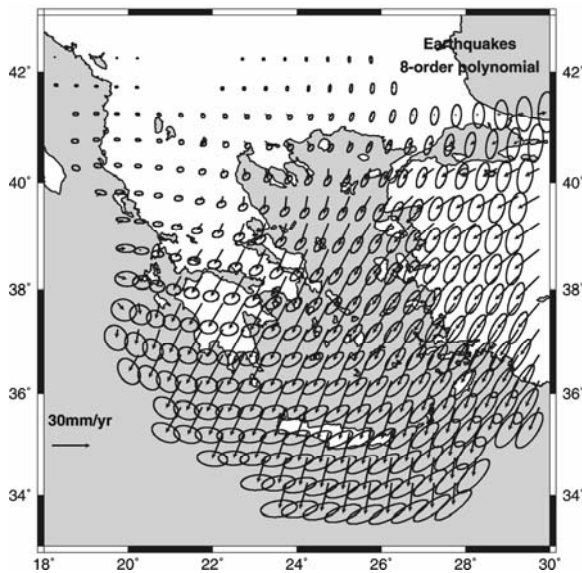


Figure 7. The continuous velocity field of the broader Aegean area relative to Europe as determined from earthquake data.

strain-rate misfit dropped to $3.0 \cdot 10^{-8}$ /yr. However, in all cases of $N > 8$ the condition number of the corresponding final linear system (equations 7) had very large condition numbers (exceeding 10^6 for the normal-equation matrix) leading to unstable solutions. Moreover, the number of polynomial coefficients increases significantly with polynomial order, without a significant reduction of the misfit. On the other hand, the relatively high polynomial order used reflects the high resolving power of the data set used in the present study, which allows the retrieval of medium-to-small scale spatial changes of the deformation.

Therefore, the simple least-squares' inversion is adequate and no special damping-smoothing constraints need to be added in the final linear system. It should also be pointed out that such constraints were already implicitly used in the seismicity parameter calculation (Papazachos, 1999a), which is the most important estimation as it affects the size of the deformation in each cell.

In general, the distribution of the estimated horizontal strain-rate tensor components show a much higher spatial variability than the GPS velocity data, requiring a higher polynomial degree. After several trials a $N=8$ order polynomial was used in order to approximate the velocity field, corresponding to a $N=7$ order polynomial for the strain-rate field with a final misfit strain-rate misfit of $3.3 \cdot 10^{-8}$ /yr. Higher polynomial degrees resulted in smaller misfits between the estimated and fitted strain rates, e.g. for $N=11$ the

Figure (7) shows the average velocity vector for each of the examined cells obtained using the random-error approach previously described. Moreover, the 1-sigma error ellipses estimated by fitting a 2-dimensional Gaussian distribution to the velocity vectors obtained for each grid cell are also shown. In general, the velocity field obtained from seismological data is quite similar with the velocity field of the original (figure 6a) or polynomially fitted (figure 6b) GPS observations. Both velocity fields are of similar magnitude order and show the same general SW direction. Moreover, additional smaller-scale characteristics are also compatible, e.g. a clockwise rotation of both velocity fields is observed for the western Greek mainland while a anticlockwise rotation is recognized in SW Turkey and the neighboring Greek islands. It should be noted that the velocity errors from the seismological data are quite large due to the large errors involved mainly in the moment-rate estimation.

3.4 Obtaining a Continuous Velocity Field From a Joint Interpretation of Seismological and GPS Data

Although the comparison of figures (6) and (7) shows many common features in the finally determined velocity fields, important differences can also be observed between the results obtained from the seismological and GPS data. Specifically, GPS velocities are in general systematically larger and in the southern Aegean the velocities obtained from the seismological data are almost N-S oriented in this area (e.g. Crete) with an angle of 20° between the two velocity vectors. The smaller-magnitude of seismological velocities show that information from GPS observations concern the total deformation in the study area, whereas seismicity data only give us the part of the deformation, which is expressed through earthquakes. Under this assumption, a comparison of the magnitude of the deformation estimated in the present study from GPS and earthquakes will allow us to find the distribution of this "efficiency index", r . Moreover, if this "efficiency index" was uniform then the velocity field determined from the seismological data would be a scaled-down version of the GPS velocity field, hence no azimuthal differences would be observed. Therefore, the observed azimuth differences previously mentioned suggest that a spatial variation of r might be expected for the study area. Moreover, it can be expected that this ratio will depend on the seismotectonic properties of each region, therefore we can reasonably assume that it exhibits a relatively smooth spatial distribution.

It is clear that the estimation of r cannot be made using velocities. In the case of earthquake data, the velocity vectors are a result of the integration of strain rates which are spatial derivatives of velocities (equations 7). In the simple 1-D case, if we denote this efficiency index as r , the velocity determined by seismicity data at distance L from the starting point where the velocity is assumed to be zero is given by:

$$u_{L_E} = \int_L \frac{\partial u_{x_E}}{\partial x} dx = \int_L \varepsilon_{xx_E} dx = \int_L r_x \varepsilon_{xx_{GPS}} dx \approx \bar{r} \int_L \varepsilon_{xx_{GPS}} dx = \bar{r} u_{L_{GPS}} \quad (8)$$

where the E and GPS subscripts denote components estimated by earthquake and GPS data, respectively, and r is the average value or the efficiency index over the range 0 to L . From this result it is clear that velocities will give us an average "efficiency" index which refers to the area between each point and the area where deformation velocities are assumed to be zero ($\varphi=43^\circ\text{N}$ in our case). Therefore, it is evident that such comparisons should be made using velocity derivatives (strain rates, vorticity, etc.).

On the basis of the previous discussion, the following relation was assumed between the strain-rate tensor components for the seismological and the GPS data-sets:

$$\dot{\varepsilon}_{ij}^E = r \dot{\varepsilon}_{ij}^{GPS} \quad i, j = x/y \quad (9)$$

where the E and GPS subscripts are similar to equation (8). Using equation (9) we can write equation (6) for the GPS data and equations (7) for the seismological data in a unified linear system of the form:

$$u_{x/y}^{GPS} = \sum_{k=1}^N \sum_{l=1}^k a_{kl}^{x/y} x^{k-l} y^l, \quad \dot{\varepsilon}_{xx}^E = r \frac{\partial u_x^{GPS}}{\partial x}, \quad \dot{\varepsilon}_{yy}^E = r \frac{\partial u_y^{GPS}}{\partial y}, \quad \dot{\varepsilon}_{xy}^E = \frac{r}{2} \left(\frac{\partial u_x^{GPS}}{\partial y} + \frac{\partial u_y^{GPS}}{\partial x} \right) \quad (10)$$

Equations (10) allows the simultaneous use of GPS and seismological data for the determination of a unique velocity field corresponding to the GPS data, u^{GPS} , as well as of the "efficiency index", r , which is also assumed to vary spatially. In the present work a low-order polynomial function, similar to equation (6), was used to describe this spatial variation of r , of the form:

$$r = \sum_{k=1}^M \sum_{l=1}^k b_{kl} x^{k-l} y^l \quad (11)$$

It should be pointed out that in order to solve the system of equations (10) there is no direct way to define the relative weight of the GPS and seismological data. In the present work we have adopted to solve system (10)

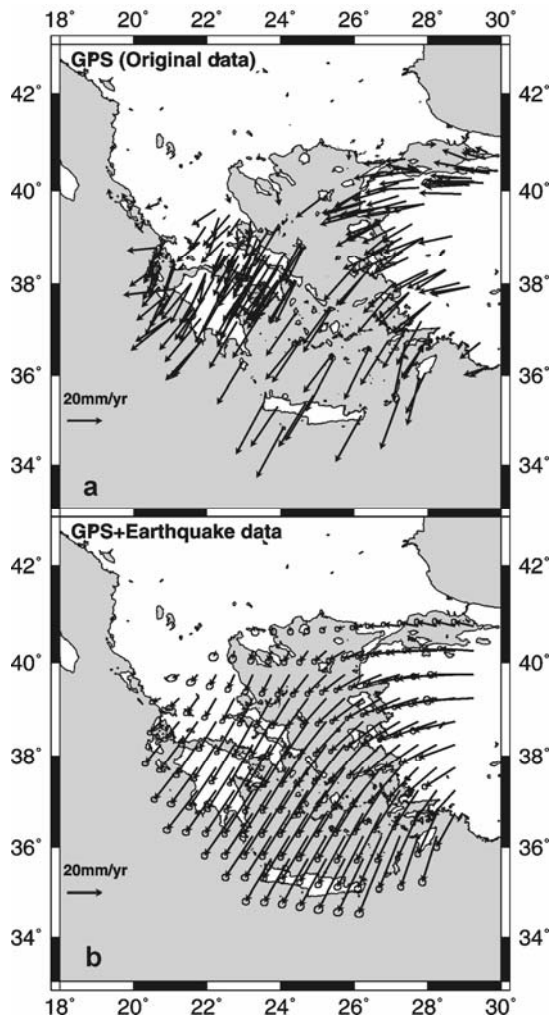


Figure 8. Comparison of (a) the GPS velocity vectors relative to Europe against (b) the final continuous velocity field obtained for the broader Aegean area relative to Europe from the joint interpretation of GPS and earthquake data. The corresponding 1-sigma error ellipses are also shown.

polynomial was used for the velocity field, in accordance with the relatively smooth spatial variability previously described for the GPS data. Also a M=3 order polynomial was used for the efficiency index r (equation 11), as higher order polynomials practically returned identical misfits for the final solution. The final misfit was 4.4mm/yr for the GPS velocities and $3.6 \cdot 10^{-8}$ /yr for the seismological strain-rates. Both values are slightly higher than misfits obtained when interpreting each data-set separately. This observation suggests that the introduction of r through equation (9) cannot explain all discrepancies between the two data sets. However, the small increase of the misfits clearly suggests that the spatial variations of r can account for the largest part of the previously observed differences between the results obtained from each individual data-set.

The finally obtained velocity field and its

using the standard Bayesian approach were all data are scaled to their a priori errors. For the GPS data (equation 10a) the observational error ellipses and corresponding covariance matrices were used to scale all equations, whereas for the earthquake data a uniform error factor of 2 (200%) was used, which corresponds to the average moment rate error which mainly controls the errors in the strain-rate estimations. Furthermore, system (10) is clearly non-linear as it is solved both for the coefficients of the $a_{kl}^{x/y}$ of the velocity field and b_{kl} of the efficiency index polynomial function. In order to solve system (10) an iterative procedure was adopted where r is initially set to 50% and system (10) was solved repeatedly until convergence.

In order to obtain reliable values for the velocity field and the efficiency index distribution, the data involved in the joint inversion of system (10) need to refer to the same study area. Therefore the inversion was limited inside the GPS data area shown in figure (6) and no grid cells with seismological strain-rate information that were located at distances larger than 80km from an original GPS observation were used. Furthermore, cells showing thrust faulting along the Hellenic Arc (cells on the outer Hellenic Arc south of latitude 38° in figure 5) were not included in the calculations as they correspond mostly to subduction events, hence may not reflect intraplate deformation. Moreover, no GPS observations were available for this thrust-faulting area.

An important point is the error assessment of the final deformation field (velocities, strain-rates, vorticities, etc.). A simple Monte Carlo approach similar to the one used for the seismological data velocity field was used and more than 2000 realizations of system (10) appropriately perturbed with random errors were solved. A N=6 order

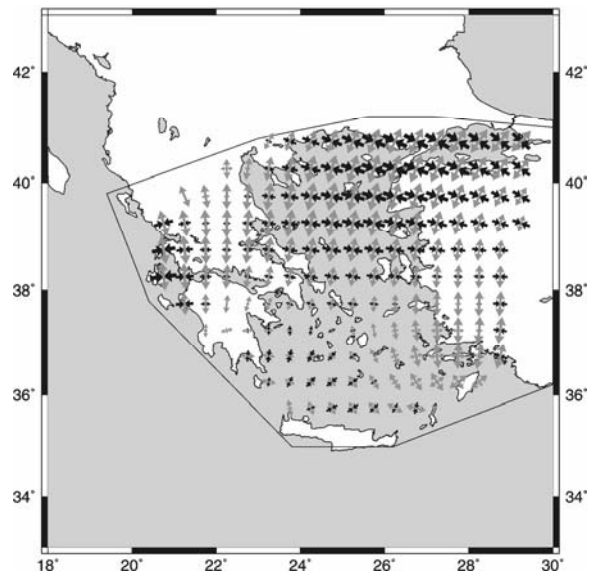


Figure 9. Distribution of the principal stress axis as these are computed from the horizontal strain-tensor components of the final velocity field, determined from the joint interpretation of earthquake and GPS data. Notice the good correlation with figure 5b.

comparison to the original GPS observations is shown in figure (8). One-sigma error ellipses obtained through the previously mentioned error analysis are also shown. A very good agreement is observed between the two figures: the joint earthquake-GPS inverted velocity field does not show the systematic discrepancies both in magnitude and orientation previously mentioned for the observed GPS data and the velocities obtained from seismological information: The rotational velocities in western Anatolia are transferred into sub-parallel velocities in central and southern Aegean, reaching up to 35mm/yr in southwestern Aegean (western Crete).

Figure (9) shows the corresponding principal axes of the unified strain-rate field. The axes are not shown in cases that the estimated azimuthal error exceeded 15°. In general the strain field shown in this figure is in quite good agreement with the pattern seen from the seismological data in figure (5b). The Northern Aegean and the western part of the North Anatolia system are dominated by strike-slip faulting (almost equal horizontal P and T vectors), which gradually changes to almost N-S extension in the Greek mainland and becomes again strike-slip in the Cephalonia island area. The extension (T) axis also shows the same pattern with the earthquake data, as it changes gradually from NNE-SSW in the northern part of eastern Aegean to NNW-SSE in the western Greek mainland. Arc-parallel extension is found close to the Hellenic Arc, although some small-magnitude compression and complicated extension patterns are also seen in the central and eastern part of southern Aegean, which are not recognized in figure (5b).

It is very interesting to study the rotational component of the obtained velocity field. While this component is the most difficult to obtain from the applied method (Holt and Haines, 1993), it is very interesting since a comparison can be made not only between earthquake and GPS data but palaeomagnetic results can also be taken into account. The vorticity component of the final velocity field is shown in figure (10a) after being reduced to degrees/15my. Clockwise rotations dominate in the Greek mainland and along the North Anatolia fault while anticlockwise rotations are observed in the western Hellenic Arc and western Turkey. In figure (10b) the most recent compilation of palaeomagnetic data available for the broader Aegean area is also presented (Kondopoulou, 2000).

The comparison between the recent (≤ 15 my) palaeomagnetic data and the results obtained in the present study shows a very good agreement between the observed rotations. Rotations up to 4°/my are observed in figure (10a) for central Greece (Corinth gulf and Peloponessus). The available palaeomagnetic data for Peloponessus (Kissel and Laj, 1988) show a dominant clockwise rotation component, which is in very good agreement with our results.

The clockwise rotation is generally well-constrained from palaeomagnetic data for post-oligocene times for the whole Ionian zone (western Greece) from the Albania borders up to the gulf of Corinth (Speranza *et al.*, 1992). This zone extends further east towards the eastern coasts of the central Greek mainland (Euboea island) with almost the same rotation pattern since late Miocene (Symeakis *et al.*, 1989) and an average rate of 2-4°/my. Both this distribution, as well as the rotation rate, is in excellent agreement with the pattern and rate (varying between 1 and 4°) found in this study from the seismological and GPS data.

To the east, in the Lesvos island, as well as in the Anatolia coast (Biga peninsula) small clockwise and anti-clockwise rotations are observed from figure (10a). Palaeomagnetic studies from this area (Kondopoulou, 1982; Kissel *et al.*, 1987) show a small clockwise rotation of the order of 1°/my or less, which partly agrees with the results obtained here. Further south (Chios and Samos islands, Bergame-Izmir area) the available palaeomagnetic data (Kissel *et al.*, 1987; Sen and Valet, 1986; Kondopoulou *et al.*, 1993) show a relative

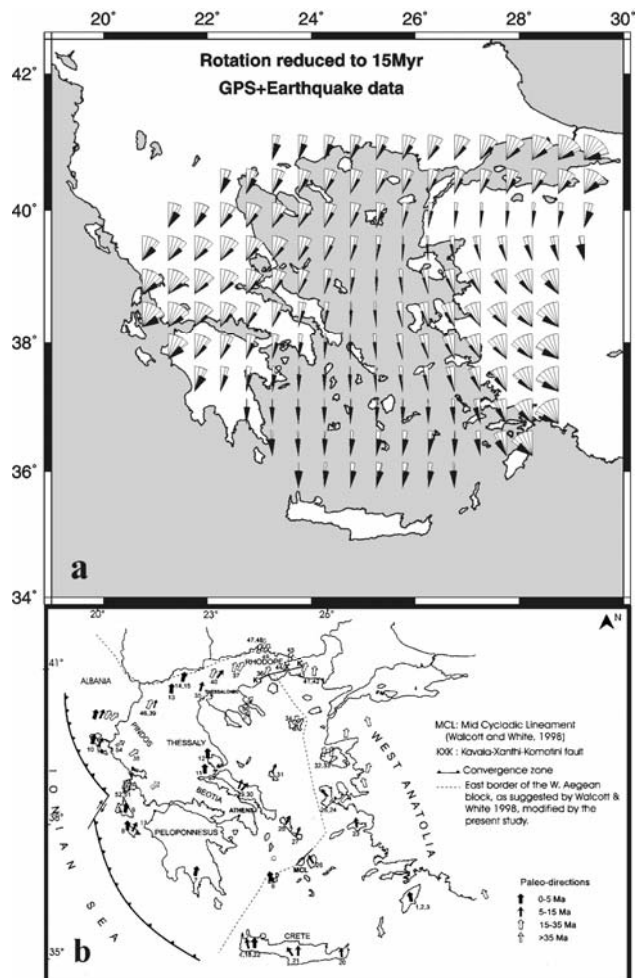


Figure 10. a) Distribution of the rotation rates and their 1-sigma errors, as these are computed from the velocity field of figure (8), after reducing them to 15my. b) Compilation of available Cenozoic palaeomagnetic rotations after Kondopoulou (2000).

complex pattern with a mixture of clockwise and anticlockwise rotations. In our results, this area represents the transition between clockwise and anticlockwise rotations, which seems to agree with the mixed rotation pattern seen in palaeomagnetic results. In the southeastern Aegean and southwestern Turkey quite large anticlockwise rotations (up to $3^\circ/\text{my}$) are found in our results from figure (10a). No robust palaeomagnetic rotations are available for the Rhodes island area. However, anticlockwise rotations are well documented (Kissel *et al.*, 1993) for the Isparta reentrant, in southwestern Turkey, which is in the southeastern corner of our study area, with an average rotation rate of $\approx 2^\circ/\text{my}$ for post-Oligocene times, in very good agreement with the $2\text{--}4^\circ/\text{my}$ seen in Figure (10a).

However, the most impressive feature of the rotations obtained from the seismological and GPS data is the boundary where the transition between clockwise and anticlockwise rotations occurs. In general, clockwise rotations dominate the western part of the Aegean, whereas anticlockwise rotations are found in the eastern

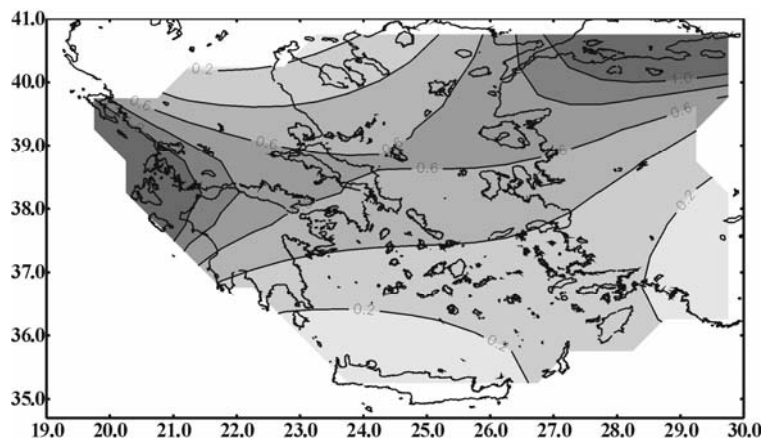


Figure 11. Distribution of the efficiency index (ratio of seismic to total deformation) for the Aegean area. Values around unity are observed for the strike-slip areas (North Anatolia Fault, Cephalonia fault), while small values ($\sim 0.2\text{--}0.4$) are observed for the rest of the Aegean region.

southern Aegean arc, in agreement with the original proposal of (Kissel and Laj, 1988) based on palaeomagnetic observations. Moreover, the boundary between the two rotations is almost identical for the part of the boundary for which recent palaeomagnetic data ($\leq 15\text{my}$) are available, which seems to cross the Aegean in a SW-NE direction, as originally proposed by *Walcott and White* (1998) and modified from *Kondopoulou* (2000) (see Figure 10b). This agreement is important if we consider the large time-extrapolation from the GPS (10-15years) and seismicity data (100-2000years) to the time-scale of the palaeomagnetic data (15my-present).

In figure (11) the spatial variation of the determined efficiency index, r , is shown. In general, the retrieved values of the efficiency index vary between ≈ 0.2 and less than 2.0. The geographical distribution of r is quite interesting: large values are observed in the areas where strike-slip faulting dominates (Cephalonia island, eastern North Aegean Trough, North Anatolia Fault), whereas low values are retrieved in the rest of the Aegean where normal faulting is mainly observed. It is interesting to notice that for the strike-slip areas almost all the deformation is released through a single main fault (e.g. Cephalonia fault, North Aegean Trough), as well as some secondary parallel branches. On the other hand, the extension field in the northern and southern Aegean is expressed through a large number of sub-parallel normal faults. The results in Figure (11) may suggest that it is easier for the accumulated strain energy to be released through earthquakes for the narrow weak fault zone of a single large fault rather than a large number of small faults. On the other hand, this result is in very good agreement with the older suggestions of *Jackson and McKenzie* (1988) who estimated the efficiency index by comparing seismic deformation with expected plate motions and who suggested a similar reduction of the seismic/total deformation ratio for the southern Aegean. The obtained results are supported by independent evidence in several areas. For example, for the Cephalonia fault seismological estimates, as well as sea-level measurements (*Papazachos et al.*, 1994) suggest a slip rate 2.5cm/yr which is almost equal to the contrast of GPS velocities across the Cephalonia fault zone. Hence, the efficiency index in this area is expected to be close to unity, as is also observed in figure (11).

4. Discussion-Conclusions

Figure (12) summarizes the results presented in the present study regarding the tecto-kinematic model that applies for the broader Aegean area. In figure (12a) the main stress-strain field characteristics are presented, as these are revealed by the information presented in figures (5) and (9). The model is very similar with the one proposed by *Papazachos et al.* (1998), where the four main zones of compression (Hellenic Arc subduction and Adriatic-western Balkan collision), strike-slip faulting (North Anatolia-North Aegean Trough and Cephalonia area), E-W extension (parallel to the compression zone) and N-S extension (most of the back-arc Aegean area) have been identified. The boundaries of these zones have been partly modified here, in accordance with the fault plane solutions and stress axes shown in figures (4), (5) and (9). It is clear that the E-W extension zone is associated with the compression zone, since the \sim N-S trending normal fault appear exclusively on the inner side (towards the back-arc area) of the compression-thrust fault area. The N-S extension dominates the back-arc area, with a NNE-SSW direction in NW Turkey (e.g. east of the Biga and Bergama area) and a NNW-SSE direction

in the western Greek mainland, as already identified by *Papazachos and Kiratzi (1996)*. In figure (12a) some of the major normal fault zones such as the Southern Thessaly zone, the Corinth gulf, the Mygdonia and Ierissos faults of the Servomacedonian massif and the Kos-Amorgos-Santorini fault zones are delineated by dashed lines. The N-S extension partly overlaps with the strike-slip zone in the Northern Aegean Trough and the westernmost part of the North-Anatolia fault, which are also shown in figure (12a), as identified on land (e.g. *Barka and Kadinsky-Cade, 1988*) and by the seismicity lineaments and corresponding fault plane solutions at sea (see figures 2 and 4).

In figure (12b) the main characteristics of the deformation velocities with respect to Europe are shown, as these are presented in figures (8) and the final model of figure (10). The study area is shown in gray and some velocity vectors (white arrows) relative to Europe are plotted, scaled according to the velocity magnitude. The rotations, as well as the isovelocity contours of the final model (figure 10) for 5, 15 and 25 mm/yr are also shown. The regional motion of the eastern Mediterranean lithosphere (*Jongsma et al., 1987*) and of the Ionian-Adriatic Sea controlled by the Adriatic (Apulia) counter-clockwise motion (*Anderson and Jackson, 1987*) are shown by large solid arrows in order to complete the picture, although it is clear that the velocity field presented here does not reflect these compressions, as it is based on GPS data on land (where extension is found) and earthquake data where thrust subduction events have not been included. On the other hand, the deformation pattern is clearly influenced by the westward motion of Anatolia. Velocities increase quite rapidly across the North Aegean Trough and the Cephalonia fault and continue to increase towards the central and southern Aegean. The average velocity in the southern Aegean relative to Europe is 30-35mm/yr. In the central part of western Anatolia, the corresponding velocity is of the order of 20-25mm/yr. This velocity increase is accompanied by a direction change of the velocity vectors, which have a large N-S component in the southern Aegean.

It is clear that this change in the velocity field should be attributed to an additional phenomenon, which occurs in the Aegean. The similarity between earthquake and GPS results (e.g. figure 6 and 7) suggests that earthquakes provide us with the key for the understanding the characteristics of the velocity field retrieved from GPS data (Figure 8a). Therefore, the change of the velocity field can be explained in the context of the stress field as this is derived from earthquake data (Figure 5), confirmed from the joint interpretation of earthquake and GPS data (Figure 9) and summarized in figure (12a). It is clear that the almost North-South extension which dominates throughout the Aegean area will increase the N-S component of the velocity field in the Aegean south of the North Aegean Trough, which will result in a direction change and an overall increase of the velocity values towards the southern Aegean. Moreover, as this extension is spread throughout the whole Aegean area, a continuous increase of the deformation velocities will be observed towards the southern Aegean, since the N-S extension components will add up, as we move away from stable Europe ($\phi=43^\circ$ N in our case). This pattern of velocity increase is also strongly supported by independent modeling results (*Meijer and Wortel, 1997*).

As far as the rotational component of the velocity field is concerned, we must notice that the obtained results

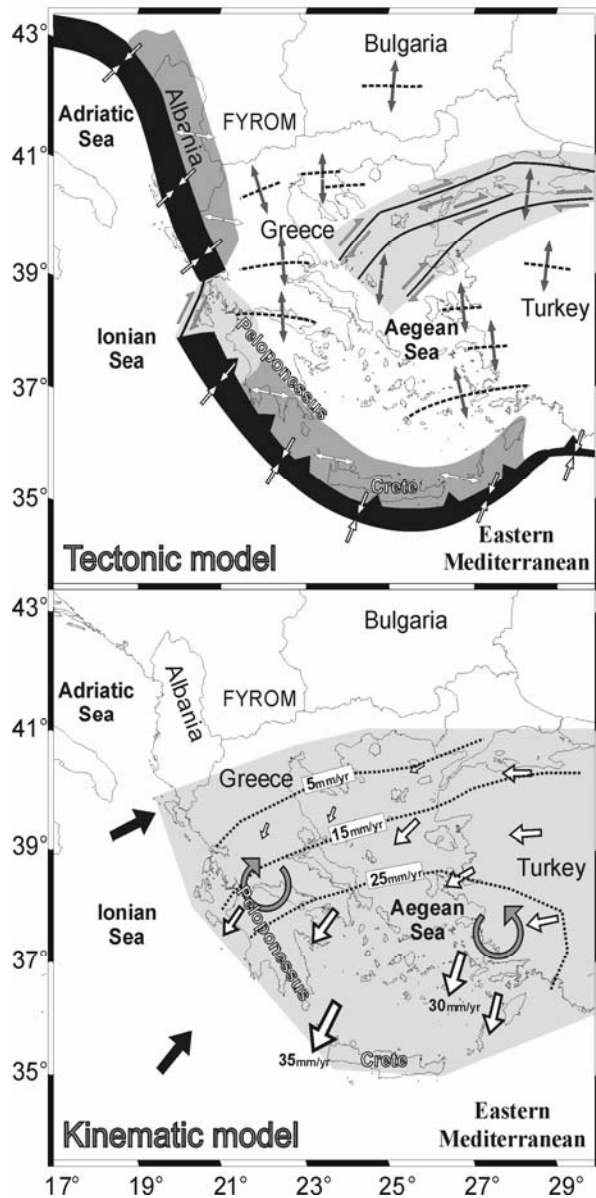


Figure 12. Final (a) tectonic and (b) kinematic model proposed for the broader Aegean area, as this is determined from the GPS and earthquake data used in the present study. Local stress field and major fault zones are shown in (a). Isovelocity contours have been drawn for the finally determined velocity field in (b). A gradual increase of velocities up to 35mm/yr is observed south of the North Anatolia Fault-North Aegean Trough and west of the Anatolia coast (see text for explanation).

from GPS and earthquake data are compatible with the general pattern of recent (≤ 15 my) palaeomagnetic rotations reported for the area. This agreement is almost surprising, considering the differences between the two data sets, both from a theoretical point of view (instantaneous rotations from GPS-earthquakes are compared with finite block rotations from palaeomagnetic data), as well as from a time-scale point of view (results from 10-2000 years are extended to 15my). However, this agreement may suggest that the presently observed geotectonic setting in the broader Aegean area is compatible with the latest phase of the on-going tectonic processes, at least for the last ~ 15 my, as this is roughly defined from the palaeomagnetic data. It is interesting to notice that the obtained rotations (clockwise for the western Aegean and the North Anatolia Fault, anticlockwise for the eastern Aegean) were not obtained in previous studies using earthquake data. *Jackson et al.* (1992) obtained a clockwise rotating field throughout the whole central and northern Aegean area, mainly due to their limited data set and their coarser grid (1.5°). These authors presented an appropriate model in order to explain and estimate how elongated features (such as some fault blocks) can perform anticlockwise rotations (e.g. in western Turkey) in a clockwise rotating field. Such arguments and assumptions about the rotating-block shape, etc. are not necessary in our case, since the obtained results show a more clear compatibility with existing palaeomagnetic estimates.

It is clear that the tecto-kinematic model presented in figure (12) is not completely novel regarding several of its aspects: The tectonic stress-strain pattern is based on previous work and the kinematic model is not very different from the models of *Papazachos* (1999b) or *McClusky et al.* (2000). However, the combined model shown in figure (12) integrates earthquake and GPS data and helps to resolve discrepancies previously observed, similar to the differences of figures (6) and (7). This is achieved through the introduction and the estimation of the efficiency index (figure 11), as well as the corresponding error analysis, which helps to match the local strains from earthquake data with the GPS data set. Of course, through this joint interpretation several additional features, such as the presence of clockwise and anticlockwise rotations are proposed or verified.

The model in figure (12) can be used to verify or argue against existing models for the Aegean area. Recent models for the Aegean (*Le Pichon et al.*, 1995; *Oral et al.*, 1995) had suggested that the Aegean is part of the a single plate, the Aegean-Anatolia microplate, which is performing an almost rigid body rotation around a pole located in the area of the Sinai peninsula (northern Africa). This model does not seem to be compatible with the results shown here, which show a more similar pattern of deformation with the original ideas of *McKenzie* (1970, 1972) and *Jackson* (1994), as also suggested by recent studies (*Papazachos*, 1999b; *McClusky et al.*, 2000). The velocity field not only increases south of the North Anatolian Fault-North Aegean Trough (which is the assumed northern boundary of the proposed Aegean microplate) but also increases from western Anatolia towards the Aegean due to the N-S extension field which is present within the Aegean area. Moreover, this extension field is the dominant mode of deformation in the area and not a second-order effect. Therefore, western Turkey and the neighboring Greek islands can be considered as a transition zone where the Anatolia rotation is "converted" to S-SW translational motion of the southern Aegean with velocities that reach up to 3.5cm/yr. On the other hand, the final velocity field shows that some internal deformation also occurs in the southern Aegean, as velocities increase from 25mm/yr in central Aegean (Euboea-Chios) to 35mm/yr or slightly larger values in the southernmost part of the Aegean (western Crete). This internal deformation, which partly contradicts the suggestion of *McClusky et al.* (2000) of a more or less rigid Peloponessus-southern Aegean block, is in agreement with the presence of the important Kos-Amorgos-Santorini seismic zone (see figure 1 and 12a), where the largest present century event in the Mediterranean Sea has occurred (Amorgos 1956 event, $M=7.5$). Unfortunately, the model in figure (12) can not help in a direct way to clarify the interpretation of the observed extensional deformation in the Aegean as a result of either the westward push of Anatolia (*McKenzie*, 1972; *Jackson*, 1994) or the Hellenic subduction roll-back (*LePichon and Angelier*, 1979; *Hatzfeld et al.*, 1997). However, it provides the basis where theoretical models, such as the ones previously mentioned (*Meijer and Wortel*, 1997) can be based in order to quantitatively estimate the effect of each factor.

It is worth noticing that the velocity field shown in Figure (12b) is in agreement with the velocity model predicted by the broken-slat model of *Taymaz et al.* (1991), as velocities increase towards the southern Aegean and clockwise and anticlockwise rotations are predicted for western and eastern Aegean, respectively. However, there is a fundamental difference between the present study and the model of *Taymaz et al.* (1991), which lies in the type of earthquake faulting that can contribute or is created by this velocity field. According to *Taymaz et al.* (1991) faults in eastern Aegean are expected to be a combination of dextral strike-slip and normal type trending NE-SW, whereas faults in western Aegean (Greek mainland) are normal with a smaller dextral strike-slip component, trending in a NW-SE direction. The results of the present study demonstrate that it is possible to retrieve an almost identical velocity field using a different type of faulting for the Greek mainland. The fault plane solutions and the stress field presented in figures (4), (5) and (9) show normal faults of a E-W up to ENE-WSW direction, that is similar to the normal fault orientation observed in eastern Aegean and the westernmost Anatolia. This type of faulting and the associated N-S/NNW-SSE extension has been well documented by a large number of normal faults in the Greek mainland, including recent events in the eastern part of central Greece (Volos 1980, $M_W=6.5$, $\zeta(\text{strike})=81^\circ$; Plataees 1981, $M_W=6.3$, $\zeta=50^\circ$; Kozani 1995, $M_W=6.6$, $\zeta=240^\circ$) for

which surface fault traces were observed and which are normal faults of E-W to NE-SW direction, occasionally with a small dextral strike-slip component. Such a stress field is supported by additional seismological and neotectonic evidence. *Caputo* (1990) found that all recent faults in the southern Thessaly basin are mostly E-W and NE-SW, whereas the NW-SE trending faults are due to an older Miocene extension field. These older NW-SE faults can still rupture in the present NNW-SSE extension field, but in this case a large sinistral strike-slip component should be expected and not a dextral or no strike-slip component as the *Taymaz et al.* model predicts. Such a sinistral component has been observed e.g. for the Atalanti normal fault which strikes in a WNW-ESE direction, as it was observed on a long surface trace of this fault that ruptured during the 1894 strong ($M=7.2$) Atalanti earthquake (*Papazachos and Papazachou*, 1997). Therefore, the dominant mode of deformation in western Aegean is similar to that of eastern Aegean, with a general E-W direction, which locally can change up to NE-SW as seen for NW Greece in figure (12a) (e.g. the Kozani 1995 earthquake). Of course, the *Taymaz et al.* model might still be applicable in certain cases and explain the presence of some secondary NNW-SSE trending normal faults in the Greek mainland.

In the present study, a good correlation has been shown to exist for the results between GPS observations and earthquakes, obtained either independently, (e.g. figures (6) and (7)) or jointly. This correlation has very important implications. The main conclusion is that deformations observed during the last decade or so (GPS data) are valid for a much longer time scale, as it is compatible with earthquake data which extend (depending on the information completeness) up to ~100-2000 years. Since this agreement can be considered to be a global-scale phenomenon, it suggests that GPS measurements can be used in combination with earthquake data not only for geotectonic modeling purposes but also for expanding our knowledge in areas where our knowledge from seismological data is poor. Moreover, valid predictions can be made on the basis of combining seismological and GPS data, through the introduction of a simple efficiency index, as previously described. In addition, interpretations based on a single data set (either earthquake or GPS data) should be made with care: Earthquake data often show less deformation that is actually taking place. On the other hand, GPS data often overestimate the seismically released deformation. Moreover, figure (11) suggests that for some areas the efficiency index, r , can take values even larger than 1, which suggests that the GPS data are not able to estimate the real long-term deformation, probably due to the limited time spanned by the GPS observations. Therefore, taking the GPS deformation as an upper limit of the real active deformation (e.g. to estimate slip rates for hazard estimation purposes) might not always be correct, though this problem will probably be solved with the gradual accumulation of more GPS observations.

As previously stated, the general agreement of rotations with recent paleomagnetic results suggest that the main features of the active deformation observed today throughout the Aegean are relatively robust characteristics of a more or less coherent tectonic phase. Therefore, the present study provides an additional motivation for future work towards the incorporation of additional geophysical and geological data for the study of the deformation field of the Aegean area. Such new data (neotectonic, palaeomagnetic, mineralogy, etc.) could be handled in a similar way either on the same space-time scale or for the study of smaller scale deformation patterns. The comparison-joint interpretation of such results with the results of this study could help to solve both important theoretical questions (e.g. generalized seismotectonic models, time variation of active deformation, etc.), as well as practical problems (e.g. more precise and robust determination of seismic hazard using seismological, geodetic, neotectonic, etc. data).

Acknowledgments. I am grateful to Prof. B. Papazachos for his continuous support and valuable comments through the preparation of this paper. This work has been partially financed by EC project ENV4-CT96-0282 and the Greek Planning and Protection Organization (OASP) projects of Research Committee of the Univ. Thessaloniki #20237 and #20321.

References

- Aki, K., and P. Richards, *Quantitative Seismology: Theory and methods*, *Freeman, San Francisco*, 557pp., 1980.
- Ambraseys, N. N., and J. A. Jackson, Seismicity and strain in the gulf of Corinth (Greece) since 1694, *J. Earth. Engin.*, 1, 433-474, 1997.
- Anderson, H., and J. Jackson, Active tectonics of the Adriatic Region, *Geophys. J. R. Astron. Soc.*, 91, 937-983, 1987.
- Armijo, R., H. Lyon-Caen, H., and D. Papanastassiou, East-west extension and Holocene normal-fault scarps in the Hellenic arc, *Geology*, 20, 491-494, 1992.
- Barka, A., and K. Kadinsky-Cade, Strike-slip faulting geometry in Turkey and its influence on earthquake activity, *Tectonics*, 7, 663-684, 1988.
- Billiris, K., D. Paradissis, G., Veis, P., England, W., Featherstone, B. Parson, P., Cross, P., Rands, M., Rayson, P., Sellers, V., Ashkenazi, M. Davison, J. Jackson, and N. Ambraseys, Geodetic determination of tectonic deformation in central Greece from 1900 to 1988, *Nature*, 350, 124-129, 1991.
- Brune, J., Seismic moment, seismicity, and rate of slip along major fault zones, *J. Geophys. Res.*, 73, 777-784, 1968.
- Caputo, R., Geological and structural study of the recent and active brittle deformation of the Neogene-Quaternary basins of Thessaly (Central Greece), Ph.D. thesis, 252 pp., Aristotle University of Thessaloniki, Thessaloniki, Greece, 1990.
- Clarke, P. J., R. R. Davies, P. C. England, B. Parsons, H. Billiris, D. Paradissis, G. Veis, P. A. Cross, P. H. Denys, V. Ashkenazi, R. Bingley, H.-G. Kahle, M.-V. Muller and P. Briole, Crustal strain in Central Greece from repeated GPS

- measurements in the interval 1989-1997, *Geophys. J. Int.*, 135, 195-214, 1998.
- Ekstrom, G., and P. England, Seismic strain rates in regions of distributed continental deformation, *J. Geophys. Res.*, 94, 10231-10257, 1989.
- Doutsos, T., and S. Kokkalas, Stress and deformation patterns in the Aegean region, *J. Struct. Geol.*, 23, 455-472, 2001.
- Fytikas, M., F. Innocenti, P. Manetti, R. Mazzuoli, A. Percerillo, and L. Vilari, Tertiary and Quaternary evolution of the volcanism in the Aegean region. In: J.E. Dixon and A.H.F. Robertson (Editors), *The Geological Evolution of the Eastern Mediterranean. Spec. Publ. Geol. Soc.*, 17, 848pp., 1985.
- Georgalas, G., Catalogue of the active volcanoes and solfatara fields in Greece, *Int. Assoc. Volcanol.*, 12, 1962.
- Gephart, J., and D. Forsyth, An improved method for determining the regional stress tensor using earthquake focal mechanism data: application to the San Fernando earthquake sequence, *J. Geophys. Res.*, 89, 9305-9320, 1984.
- Haines, A. J., Calculating velocity fields across plate boundaries from observed shear rates, *Geophys. J. R. Astron. Soc.*, 68, 203-209, 1982.
- Haines, A. J., and W. E. Holt, A procedure for obtaining the complete horizontal motions within zones of distributed deformation from inversion of strain rate data, *J. Geophys. Res.*, 98, 12057-12082, 1993.
- Hatzfeld, D., G. Pedotti, P., Hatzidimitriou, D., Panagiotopoulos, M., Scordilis, J., Drakopoulos, K., Makropoulos, N., Delibasis, J., Latoussakis, J., Baskoutas, and M. Frogneux, The Hellenic subduction beneath the Peloponnesse: First results of a microearthquake study, *Earth. Planet. Sci. Lett.*, 93, 283-291, 1988.
- Hatzfeld, D., J. Martinod, G. Bastet and P. Gautier, An analog experiment for the Aegean to describe the contribution of gravitational potential energy, *J. Geophys. Res.*, 102, 649-659, 1997.
- Holt, W. E., J. F. Ni, T. C. Wallace, and A. J. Haines, The active tectonics of the eastern Himalayan syntaxis and surrounding regions, *J. Geophys. Res.*, 96, 14595-14632, 1991.
- Holt, W. E., and A. J. Haines, Velocity fields in deforming Asia from the inversion of earthquake-released strains, *Tectonics*, 12, 1-20, 1993.
- Jackson, J., Active tectonics of the Aegean region, *Annu. Rev. Earth Planet. Sci.*, 22, 239-271, 1994.
- Jackson, J. A., and D. P. McKenzie, The relationship between plate motions and seismic moment tensors, and the rates of active deformation in the Mediterranean and the Middle East, *Geophys. J. R. Astron. Soc.*, 93, 45-73, 1988.
- Jackson, J., J. Haines, and W. Holt, The horizontal velocity field in the deforming Aegean Sea region determined from the moment tensors of earthquakes, *J. Geophys. Res.*, 97, 17657-17684, 1992.
- Jongsma, D., J. Woodside, G.C.P. King, and J.E. Van Hintta, The Medina Wrench: A key to the kinematics of the central and eastern Mediterranean over the past 5 Ma, *Earth. Planet. Sci. Lett.*, 82, 87-106, 1987.
- Kahle, H.-G., M. V. Muller, A. Geiger, G. Danuser, S. Mueller, G. Veis, H. Billiris, and D. Paradisis, The strain field in NW Greece and the Ionian islands: Results inferred from GPS measurements, *Tectonophysics*, 249, 41-52, 1995.
- Kahle, H.-G., C. Straub, R. Reilinger, S. McClusky, R. King, K. Hurst, G. Veis, K. Kastens, and P. Cross, The strain field in the eastern Mediterranean estimated by repeated GPS measurements, *Tectonophysics*, 294, 237-252, 1998.
- Kiratzis, A. A., E. E. Papadimitriou, and B. C. Papazachos, A microearthquake survey in the Steno dam site in northwestern Greece, *Annales Geophysicae*, 5, 161-166, 1987.
- Kissel, C., and C. Laj, The tertiary geodynamic evolution of the Aegean arc: a palaeomagnetic reconstruction, *Tectonophysics*, 146, 183-201, 1988.
- Kissel, C., C. Laj, A. M. C. Sengor, and A. Poisson, Palaeomagnetic evidence for rotation of opposite senses of adjacent blocks in the northeastern Aegean and western Anatolia, *Geophys. Res. Lett.*, 14, 907-910, 1987.
- Kissel, C., O. Averbuch, D. Frizon de Lamotte, O. Monod, and S. Allerton, First Palaeomagnetic evidence for a post-Eocene clockwise rotation of the Western Taurides thrust belt east of the Isparta reentrant (Southwestern Turkey), *Earth. Planet. Sci. Lett.*, 117, 1-14, 1993.
- Kondopoulou, D., Palaeomagnetism et deformations neogenes du Nord de la mer Egee, Thesis, Univ. of Strasbourg, 1982.
- Kondopoulou, D., Palaeomagnetism in Greece: Cenozoic and Mesozoic components and their geodynamic implications, *Tectonophysics*, 326, 131-151, 2000.
- Kondopoulou, D., V. Leci, and C. Symeakis, Palaeomagnetic study of the tertiary volcanics in Chios island (Greece), *Proc. of the 2nd Congress of the Hellenic Geophysical Union, Florina, Greece, 5-7 May, 2-3*, 676-687, 1993.
- Kostrov, V. V., Seismic moment and energy of earthquakes, and seismic flow of rock, *Izv. Acad. Sci. USSR Phys. Solid Earth*, 1, 23-44, 1974.
- Le Pichon, X., and J. Angelier, The Hellenic arc and trench system: a key to the neotectonic evolution of the eastern Mediterranean area, *Tectonophysics*, 60, 1-42, 1979.
- Le Pichon, X., N. Chamot-Rooke, S. Lallemand, R. Noomen, and G. Veis, Geodetic determination of the kinematics of central Greece with respect to Europe: Implications for eastern Mediterranean tectonics, *J. Geophys. Res.*, 100, 12675-12690, 1995.
- Makris, J., A dynamic model of the Hellenic arc deduced from geophysical data, *Tectonophysics*, 36, 339-346, 1976.
- Makris, J., The crust and upper mantle of the Aegean region from deep seismic soundings, *Tectonophysics*, 46, 269-284, 1978.
- McClusky, S., S. Balassanian, A. Barka, C. Demir, S. Ergintav, I. Georgiev, O. Gurkan, M. Hamburger, K. Hurst, H. Kahle, K. Kastens, G. Kekelidze, R. King, V. Kotzev, O. Lenk, S. Mahmoud, A. Mishin, M. Nadariya, A. Ouzounis, D. Paradisis, Y. Peter, M. Prilepin, R. Reilinger, I. Santli, H. Seeger, A. Teled, M.N. Toksoz, and G. Veis, Global Positioning System constraints on plate kinematics and dynamics in the eastern Mediterranean and Caucasus, *J. Geophys. Res.*, 105, 5695-5719, 2000.
- McKenzie, D., Plate tectonics of the Mediterranean region, *Nature*, 226, 239-243, 1970.
- McKenzie, D., Active tectonics of the Mediterranean region, *Geophys. J. R. Astron. Soc.*, 30, 109-185, 1972.
- McKenzie, D.P., Active tectonics of the Alpine-Himalayan belt: The Aegean sea and surrounding regions, *Geophys. J. R. Astron. Soc.*, 55, 217-254, 1978.

- Meijer, P.T., and M.J.R., Wortel, Present-day dynamics of the Aegean region: A model analysis of the horizontal pattern of stress and deformation, *Tectonics*, 16, 879-895, 1997.
- Milne, W., and A. Davenport, Determination of earthquake risk in Canada, *Bull. Seismol. Soc. Am.*, 59, 729-754, 1969.
- Molnar, P., Earthquake recurrence intervals and plate tectonics, *Bull. Seismol. Soc. Am.*, 69, 115-133, 1979.
- Moritz, H., Advanced Physical Geodesy, Wichmann Verlag, 500pp., 1980.
- Oral, M. B., Global Positioning System (GPS) measurements in Turkey (1988-1992): Kinematics of the Africa-Arabia-Eurasia plate Collision Zone, Ph.D. thesis, 344 pp., MIT, March 1994.
- Oral, M. B., R. E. Reilinger, M. N. Toksoz, R. W. King, A. A. Barka, and I. Kinik, Coherent plate motions in the eastern Mediterranean continental collision zone, 76, 9-11, 1995.
- Papazachos, B.C., Seismicity of the Aegean and surrounding area, *Tectonophysics*, 178, 287-308, 1990.
- Papazachos, B. C., and N. D. Delibasis, Tectonic stress field and seismic faulting in the area of Greece, *Tectonophysics*, 7, 231-255, 1969.
- Papazachos, B. C., and P. E. Comninakis, Geophysical features of the Greek island arc and the Eastern Mediterranean ridge, *Proc. C. R. Seances de la Conference Reunie a Madrid*, 16, 74-75, 1969.
- Papazachos, B. C., and P. E. Comninakis, Geophysical and tectonic features of the Aegean arc, *J. Geophys. Res.*, 76, 8517-8533, 1971.
- Papazachos, B. C., A. Kiratzi, P. Hatzidimitriou, and A. Rocca, Seismic faults in the Aegean area, *Tectonophysics*, 106, 71-85, 1984.
- Papazachos, B. C., G. F. Karakaisis, and P. M. Hatzidimitriou, Further information on the transform fault of the Ionian sea, *Proc. XXIV Gen. Ass. Europ. Seism. Com., Athens, 19-24 September*, 1994.
- Papazachos, B. C., and C. Papazachou, The earthquakes of Greece, *Ziti Publ., Thessaloniki, Greece*, 304pp., 1997.
- Papazachos, B. C., B. Karakostas, E. Scordilis, C. B. Papazachos, Ch. Papaioannou, and G. Karakaisis, Shallow seismicity of Greece, *IASPEI 29th General Assembly, Thessaloniki, 18-28 August*, 1997.
- Papazachos, B.C., E.E. Papadimitriou, A.A. Kiratzi, C.B. Papazachos, and E.K. Louvari, Fault plane solutions in the Aegean sea and the surrounding area and their tectonic implications, *Boll. Geof. Teor. Appl.*, 39, 199-218, 1998.
- Papazachos, B. C., Ch. Papaioannou, C. B. Papazachos, and A. S. Savvaidis, Rupture zones and seismic faults of shallow earthquakes in Greece, *Tectonophysics*, 308, 205-221, 1999.
- Papazachos, B. C., V. G. Karakostas, C. B., Papazachos, and E. M. Scordilis, The geometry of the Wadati-Benioff zone and lithospheric kinematics in the Hellenic arc, *Tectonophysics*, 319, 275-300, 2000.
- Papazachos, C. B., An alternative method for a reliable estimation of seismicity with an application in Greece and the surrounding area, *Bull. Seismol. Soc. Am.*, 89, 111-119, 1999a.
- Papazachos, C. B., Seismological and GPS evidence for the Aegean-Anatolia interaction, *Geophys. Res. Lett.*, 17, 2653-2656, 1999b.
- Papazachos, C. B., and A. A. Kiratzi, A formulation for reliable estimation of active crustal deformation and its application to central Greece, *Geophys. J. Int.*, 111, 424-432, 1992.
- Papazachos, C. B., and A. A. Kiratzi, A detailed study of the active crustal deformation in the Aegean and surrounding area, *Tectonophysics*, 253, 129-153, 1996.
- Papazachos, C. B., and G. Nolet, P and S deep velocity structure of the Hellenic area obtained by robust non-linear inversion of travel times, *J. Geophys. Res.*, 102, 8349-8367, 1997.
- Pavlidis, S., Active faults in Greece, *J. Earth. Prediction and Res.*, 5, 422-430, 1996.
- Reilinger, R. E., S. C. McClusky, M. B. Oral, R. W. King, M. N. Toksoz, A. A. Barka, I. Kinik, O., Lenk, and I. Sanli, Global Positioning System measurements of present-day crustal movements in the Arabia-Africa-Eurasia plate collision zone, *J. Geophys. Res.*, 102, 9983-9999, 1997.
- Scordilis, E. M., G. F. Karakaisis, B. G. Karakostas, D. G. Panagiotopoulos, P. E. Comninakis, and B. C. Papazachos, Evidence for transform faulting in the Ionian Sea: the Cephalonia island earthquake sequence of 1983, *Pure Appl. Geophys.*, 123, 388-397, 1985.
- Sen, S., J. P., Valet, Magnetostratigraphy of late Miocene continental deposits in Samos, Greece, *Earth. Planet. Sci. Lett.*, 80, 167-174, 1986.
- Spakman, W., Upper mantle delay time tomography with an application to the collision zone of the Eurasian, African and Arabian plates, Ph.D. thesis, 200 pp., Univ. of Utrecht, Utrecht, Netherlands, 1988.
- Speranza, F., C. Kissel, I. Islami, A. Hyseni, and C. Laj, First palaeomagnetic evidence for rotation of the Ionian zone of Albania, *Geophys. Res. Lett.*, 19, 697-700, 1992.
- Straub, C., Recent crustal deformation and strain accumulation in the Marmara Sea region, N.W. Anatolia, inferred from GPS measurements, Ph.D. thesis, 184 pp., ETH Zurich-Switzerland, July 1996.
- Straub, C., H.-G. Kahle, and C. Schindler, GPS and geologic estimates of the tectonic activity in the Marmara Sea region, N.W. Anatolia, *J. Geophys. Res.*, 102, 27587-27601, 1997.
- Symeakis, C., J. L. Mercier, P. Vergely, and C. Kissel, Late Cenozoic rotations along the N.Aegean Trough fault zone (Greece): Structural constraints, In Kissel and Laj, eds. *Palaeomagnetic rotations and continental deformation*, Kluwer Publ., 131-143, 1989.
- Taymaz, T., J. Jackson, and D. McKenzie, Active tectonics of the north central Aegean Sea, *Geophys. J. Int.*, 106, 433-490, 1991.
- Tselentis, G., and C. Makropoulos, Rates of crustal deformation in the gulf of Corinth (central Greece) as determined from seismicity, *Tectonophysics*, 124, 55-66, 1986.
- Voght, P., and P. Higgs, An aeromagnetic survey of the eastern Mediterranean sea and its interpretation, *Earth. Planet. Sci. Lett.*, 5, 439-448, 1969.
- Walcott, C., and S. White, Constraints on the kinematics of post-orogenic Extension imposed by stretching lineations in the Aegean region, *Tectonophysics*, 298, 155-175, 1998.

Table 1. Azimuth, ζ° , and plunge, δ° , of the P and T axes of the 39 clusters (CL) of earthquakes from the Aegean area, modified from Papazachos et al. (1999).

CL	φ° N	λ° E	P		T		CL	φ° N	λ° E	P		T		CL	φ° N	λ° E	P		T	
			ζ°	δ°	ζ°	δ°				ζ°	δ°	ζ°	δ°				ζ°	δ°		
A1	42.05	19.00	231	27	54	63	T1	42.12	24.76	216	86	4	3	T14	39.21	29.78	146	87	16	2
A2	40.98	19.78	242	16	104	69	T2	41.82	23.00	271	90	181	0	S1	40.76	29.64	138	51	44	3
A3	39.31	20.73	242	2	352	84	T3	40.81	23.69	319	86	168	4	S10	38.68	20.59	234	14	331	26
H1	37.30	20.77	229	21	25	67	T4	40.51	21.88	257	86	151	1	S11	38.17	20.28	263	14	1	29
H2	35.91	21.02	205	13	14	76	T5	39.24	22.65	201	87	354	3	S12	37.77	20.72	246	24	355	37
H3	35.06	23.60	211	29	21	61	T6	38.33	22.24	322	79	181	8	S2	40.30	28.46	112	32	22	0
H4	34.50	24.90	184	28	11	62	T7	38.63	24.04	288	76	191	2	S3	40.38	25.92	282	38	22	12
H5	35.00	27.33	202	14	6	76	T8	38.12	23.17	319	88	161	2	S4	39.62	24.16	96	18	187	4
H6	36.30	28.90	29	5	287	67	T9	36.65	26.35	77	84	324	2	S5	39.08	24.89	270	13	178	9
M1	41.16	20.41	207	67	97	8	T10	37.46	28.27	253	83	1	2	S6	38.79	25.72	111	15	19	9
M2	39.76	20.98	315	84	105	5	T11	37.56	29.51	159	80	350	10	S7	37.68	26.95	80	80	188	3
M3	36.35	22.85	112	78	285	11	T12	38.36	28.70	263	78	22	6	S8	38.50	26.54	94	74	188	1
M4	35.27	26.67	265	82	108	8	T13	39.28	28.52	231	82	11	6	S9	37.69	21.57	92	30	359	6